Modelling of agro-zootechnical anaerobic co-digestion for full-scale applications: Digital Supplementary Material

Davide Carecci[1], Giulia Quarta[1], Arianna Catenacci[2], Gianni Ferretti[1], Elena Ficara[2]

In the following, ***bold*** is used to differentiate vectors and matrix from scalars. The $\odot$ symbol refers to the Hadamard (element-wise) product between vectors.

I. The "high-fidelity" model: agri-AcoDM as an extended ADM1

The high-fidelity model that was considered, referred to as 'agri-AcoDM', is an extension of ADM1 that resulted in a strongly non-linear differential algebraic equation (DAE) system with 43 state variables. The majority of the extensions are described in detail in other works [6], [5], [12] and are briefly listed hereafter:

- the disintegration step was removed;
- three carbohydrates (X_{ch}) and two proteins (X_{pr}) with different hydrolyzing behaviors (readily (r), mildly (m), and slowly (s) available) have been added [5]. Although the number of state variables was increased, hydrolysis was still modeled as first-order process;
- dead bacterial biomass (X_{dec}) and lignin (X_{lig}) were added, as these components display significantly different chemical oxygen demand to volatile solids (COD/VS) stoichiometric ratio compared to the original sole non-biodegradable particulate (X_i);
- precipitation/dissolution processes were modeled similarly to [2], and 4 salts have been added to grasp the fate of total ammoniacal nitrogen N (TAN, S_{in}), inorganic dissolved carbon C (S_{ic}) and phosphorous P (S_{ip}), modeled as in [12];
- to effectively capture precipitation processes, activity corrections to account for the non-ideality of the liquid bulk were added into the acid-base physico-chemical equations;
- although a pH drop associated to a VFA accumulation is the main cause of methanogenesis inhibition, high VFA concentrations themselves were shown to have an inhibitory effect [10]. The large delay in the VFA to pH dynamics, especially in well-buffered systems, suggests that pH alone is unlikely to be the primal cause of inhibition. For this reason, the Monod-like functions traditionally used for the methane production kinetics were replaced with Haldane-like ones [9].

The overall differential algebraic equation system is defined as Eq. (1), where $\mathbf{x}$ are dynamic state variables (mainly concentrations of chemical compounds and bacteria populations), $\mathbf{z}$ are algebraic variables (mainly physico-chemical quantities), $\mathbf{u}$ are inputs, $\boldsymbol{\theta}$ are parameters and $\mathbf{y}$ are measurable outputs. Functions $\mathbf{f}$ and $\mathbf{g}$ are highly non-linear (and in some cases $\in C^0$).

$$\begin{cases} \dot{\mathbf{x}} = \mathbf{f}(\mathbf{x},\mathbf{z},\mathbf{u},\boldsymbol{\theta}) \\ \mathbf{0} = \mathbf{g}(\mathbf{x},\mathbf{z},\mathbf{u},\boldsymbol{\theta}) \\ \mathbf{y} = \mathbf{h}(\mathbf{x},\mathbf{z},\mathbf{u},\boldsymbol{\theta}) \end{cases} \tag{1}$$

The vector of parameters $\boldsymbol{\theta}$ is partitioned into $\boldsymbol{\theta_{in,i}}$, representing the concentration (g L^{-1}) of state variables in the i^{th} co-feedstock (for each of the n co-feedstocks in the input flux i.e. $i = 1...n$), and $\boldsymbol{\theta_p}$, namely stoichiometric, physico-chemical and kinetic parameters (actually a function of process temperature, that is usually almost constant in full-scale applications). An example of ODE for the liquid-solid mixture mass balances is Eq.(2), i.e.;

$$\begin{aligned} \dot{\mathbf{x}} &= \frac{\sum_{i=1}^{n} u_i}{V}(\mathbf{x_{in}} - \mathbf{x}) + \mathbf{K}_G \mathbf{r}(\mathbf{x},\boldsymbol{\theta}_p,\mathbf{z}) \\ x_{in}^{(j)} &= \frac{\sum_{i=1}^{n} u_i \theta_{in,i}^{(j)}}{\sum_{i=1}^{n} u_i}, \qquad j \in \mathbf{x} \end{aligned} \tag{2}$$

where V (m^3) is the reactor volume, u_i (m^3 d^{-1}) is the volume flowrate of the i^{th} input co-feedstock, $\mathbf{K}_G$ is the transposed stoichiometric Gujer matrix that guarantees COD and mass conservation (C, N, P), extended and modified according to the new variables and processes introduced and $\mathbf{r}$ the vector of process kinetic rates. An example of model non-linearities is shown in Eq. (3), that defines the gross growth reaction rate r_{ac} of the acetoclastic methanogens population (X_{ac}) via acetate uptake, i.e.,

$$r_{ac} = k_{\max,ac} f_{\mathrm{pH}} \frac{K_{I,nh3}}{K_{I,nh3} + S_{nh3}} \frac{S_{ac}}{K_{s,ac} + S_{ac} + \frac{S_{ac}^2}{K_{I,hac,ac}}} \min_j \left(\frac{S_j}{S_j + K_{s,j}} \right) X_{ac} \tag{3}$$

where $k_{\max,ac}$ (g_{CODs} g_{CODx}^{-1} d^{-1}) is the maximum specific bacterial growth constant and f_{pH} is the function that describes pH dependency [3]. The inhibition constant for free ammonia concentration (S_{nh3}) is $K_{I,nh3}$ (mol_N L^{-1}) and $K_{s,j}$ (g_{COD_s} L^{-1}) is the half-saturation constant for the limiting nutrient S_j ($j = \{P,N\}$) [3]. The maximum growth, inhibition ($K_{I,hac,ac}$ (g_{COD_s} L^{-1})) and half-saturation ($K_{s,ac}$) constants define the shape of the Haldane-like function for total acetate concentration (S_{ac}) uptake. For gaseous states, Eq. (2) still holds and has a null influent contribution, V is

the reactor head-space volume and u_i is the biogas outflow, regulated by a SISO PI controller that keeps it slightly over atmospheric pressure. The gas/liquid transfer kinetics are described according to the Fick's law. The much faster acid-base physico-chemical reactions have been modeled as an algebraic equation system ($\mathbf{z} \in \mathbb{R}^{30}$) [2]. The agri-AcoDM was implemented using Modelica, an open-source, high-level, declarative and object-oriented modeling language, and employing the free OpenModelica interpreter [13].

II. The "reduced-order" models: AM2HN and AM2HNtan as extended AM2

Since inhibition from free ammonia (S_{nh3}) released by N-rich co-feedstocks (e.g. animal slurries) can be relevant [19], [25], two model versions with ('AM2HNtan') and without ('AM2HN') S_{nh3} inhibition were studied.

$$\begin{cases} \dot{\mathbf{x}} = \mathbf{f}(\mathbf{x}, \mathbf{u}, \boldsymbol{\theta}) \\ \mathbf{y} = \mathbf{h}(\mathbf{x}, \mathbf{u}, \boldsymbol{\theta}) \end{cases} \tag{4}$$

The ordinary differential equation (ODE) system is defined as Eq. (4) (with rational non-linear $\mathbf{f}$ and $\mathbf{h}$) and described hereafter. The AM2HNtan model is described by Eq.s (5)-(25). With respect to the original AM2HN model version, the $\mathbf{X_h}$ ($g_{VS}\ L^{-1}$) was extended from a single state variable to a vector $\in \mathbb{R}^n$, and the N state was added: the former describes the dynamics of the biodegradable particulate fraction of each co-feedstock, whereas the latter describes the dynamics of the TAN concentration in the bulk.

$$\dot{\mathbf{X}}_\mathbf{h} = D(\mathbf{X}_{\mathbf{h},\mathbf{in}} - \alpha \mathbf{X}_\mathbf{h}) - \mathbf{k}_\mathbf{h} \odot \mathbf{X}_\mathbf{h} \tag{5}$$

$$\dot{X}_1 = (\mu_1 - \alpha D - k_{d,1}) X_1 \tag{6}$$

$$\dot{X}_2 = (\mu_2 - \alpha D - k_{d,2}) X_2 \tag{7}$$

$$\dot{S}_1 = D(S_{1,in} - S_1) - k_1 \mu_1 X_1 + + \sum_{i=1}^{n} (COD_{X_h}/VS_{X_h})_i k_{h,i} X_{h,i} \tag{8}$$

$$\dot{S}_2 = D(S_{2,in} - S_2) + k_2 \mu_1 X_1 - k_3 \mu_2 X_2 \tag{9}$$

$$\dot{Z} = D(Z_{in} - Z) + \sum_{i=1}^{n} N_{X_{h,i}} k_{h,i} X_{h,i} - - N_x[(\mu_1 - k_{d,1}) X_1 + (\mu_2 - k_{d,2}) X_2] \tag{10}$$

$$\dot{C} = D(C_{in} - C) + k_4 \mu_1 X_1 + k_5 \mu_2 X_2 - qC \tag{11}$$

$$\dot{N} = D(N_{in} - N) + \sum_{i=1}^{n} N_{X_{h,i}} k_{h,i} X_{h,i} - - N_x[(\mu_1 - k_{d,1}) X_1 + (\mu_2 - k_{d,2}) X_2] \tag{12}$$

$$y_1 = qM = k_6 \mu_2 X_2 \tag{13}$$

$$y_2 = qC = k_L a (CO_2 - k_H P_c) \tag{14}$$

where:

$$D = \frac{\sum_{i=1}^{n} u_i}{V} \tag{15}$$

$$\mu_1 = \mu_{max,1} \frac{S_1}{S_1 + K_{s,1}} \tag{16}$$

$$\mu_2 = \mu_{max,2} \frac{S_2}{S_2 + K_{s,2} + \frac{S_2^2}{K_{I,2}}} \left(\frac{K_{I,nh3}}{K_{I,nh3} + S_{nh3}} \right) \tag{17}$$

$$CO_2 = C + S_2 - Z \tag{18}$$

$$\phi = CO_2 + k_H P_t + \frac{qM}{k_L a} \tag{19}$$

$$Pc = \frac{\phi - \sqrt{\phi^2 - 4 k_H P_t CO_2}}{2 k_H} \tag{20}$$

$$pH = -\log_{10} \left(\frac{K_{a,co2} CO_2}{Z - S_2} \right) \tag{21}$$

$$S_H^+ = \left(\frac{1}{10} \right)^{pH} \tag{22}$$

$$S_{nh3} = \frac{K_{a,nh4} N}{K_{a,nh4} + S_H^+} \tag{23}$$

$$x_{in}^{(j)} = \frac{\sum_{i=1}^{n} u_i \theta_{in,i}^{(j)}}{\sum_{i=1}^{n} u_i}, \qquad j \in \{S_1, S_2, Z, C, N\} \tag{24}$$

$$\mathbf{X}_{\mathbf{h},\mathbf{in}} = \frac{\mathbf{u} \odot \mathbf{BD}_{\mathbf{vs_p}} \odot \mathbf{VS_p}}{\sum_{i=1}^{n} u_i} \tag{25}$$

To simulate the carbon dioxide flow rate (qC) and exploit its measurement, the model incorporates both total alkalinity (Z) and inorganic dissolved carbon (C) states. Due to the low dilution ratios (D) typical of the operations of agro-zootehnical AcoD, bacterial decay and inorganic N release were considered too. The biodegradability ($\mathbf{BD_{vs_p}}$) of the particulate fraction (p subscript) of the volatile solids ($\mathbf{VS_p}$) of each co-feedstock is a vector with n entries fixed as constants and computed from the time-average chemical and biochemical characterizations [6]. Same holds for the N concentration ($\mathbf{N_{X_h}}$) and the COD over VS ratios ($\mathbf{COD_{X_h}/VS_{X_h}}$) of $\mathbf{X_h}$. Similarly, each entry of $\boldsymbol{\theta_{in,i}}$ is set from feedstock's characterization, but it can be time-varying and its flow-weighted average is used to compute the corresponding entry of the reactor's influent vector of $\mathbf{x_{in}}$ (Eq. (24)). The values of other parameters such as the biomass N content (N_x) and the physico-chemical equilibrium constants were taken from the original ADM1 values (corrected with the actual process temperature). Unit density for the solid-liquid organic mixtures (feedstocks and digestate) was considered. The parameter α (i.e. the ratio between the particulate and soluble matter retention times) was set to unity. For the description of all other quantities the reader is referred to the original AM2 manuscript. The unit of each quantity is usually the same of the original AM2 manuscript and when units differ, they can be intended from Table I (and Table II in the main manuscript, where parameters are reported). In the 'AM2HN' version, the N state equation is not present and the μ_2 expression is reduced to the sole original Haldane function for VFA.

Constants: $\mathbf{COD_{X_h}/VS_{X_h}}$ = [1.27, 1.49, 1.39] $g_{COD}\ g_{VS}^{-1}$;

$\mathbf{N_{xh}}$ = [0.89, 1.53, 7.34] mmol$_N$ g$_{VS}^{-1}$; N_x = 8.58 mmol$_N$ g$_{VS}^{-1}$; $K_{a,nh4}$ = 1.85e^{-9} mmol L^{-1}; $K_{a,co2}$ = 5.08e^{-7} mmol L^{-1}; k_H = 22.7 mmol L^{-1} atm^{-1}.

III. Parameter estimation

Figure 1 gives a schematic representation of the general modeling approach that was followed to derive a control-oriented model suitable for full-scale applications (it is an attempt to summarize the content of Sections IV) and III.

A. Parameter subset selection (PSS)

The agri-AcoDM simulation was started one month before the actual start of the dataset considered for training/testing, to exclude the initial inoculum adaptation phase. The initial conditions were set equal to steady-state values from a simulation with the constant input equal to the initial diet that was fed during the period of inoculum adaptation and before the diet change i.e. from 25/10/2023 until 05/02/2024 (see Table II and Section IV).

In addition to the 24 most uncertain kinetic parameters ($\boldsymbol{\theta_p}$), selected based on literature [19], other 18 $\boldsymbol{\theta_{in,i}}$ ($i = 1...n$) were selected to conduct the sensitivity analyses, for a total of 78 parameters ($n = 3$). Since a comprehensive organic characterization was carried out at least once for each of the i^{th} co-feedstock, no $\boldsymbol{\theta_{in,i}}$ were considered for estimation given their much lower range of uncertainty with respect to $\boldsymbol{\theta_p}$. Indeed, the overall $BD_{vs,i}$ were computed from the asymptotic value of the BMP tests ($BMP_{\infty,i}$), whereas literature/hypothesized values were set for the $BD_{vs,i}$ fractioning among the different macromolecule's contributions (e.g. carbohydrates, proteins, lipids) [24].

The local (L.)/once-at-a-time dynamic sensitivity analysis was computed as '3-point finite-differences', whereas Sobol's first-order indexes were considered to compute the global (G.)/multiple-at-a-time dynamic sensitivity, using the python SALib package [16]. The relevant model non-linearity makes the latter more suited than local/linear analysis (that strongly depends on the *nominal* start values of $\boldsymbol{\theta_p}$). However, as it entails some drawbacks as well, both analyses were compared. Two main drawbacks are (i) the high computational burden to guarantee convergence and (ii) the risk of biased results when crossing certain regions of the parameter space (e.g. bifurcation given by the Haldane inhibition) [20]. The computation of the relative-relative sensitivity matrices ($\mathbf{SI_{rr}}$) and the related analogous of the $\boldsymbol{FIM}$ based on global sensitivity analysis (Global Sensitivity Information Matrix $\boldsymbol{GSIM}$) was previously carried out in [1]. The main drawbacks of the PSS proposed by [4] are: (i) it is based on local sensitivity (i.e. it depends on the *nominal* initial values of $\boldsymbol{\theta_p}$), (ii) the high dependence of the outcome to user-set hyperparameters (e.g. collinearity index (γ) upper threshold) [18], and (iii) it becomes computationally expensive when the dimension of $\boldsymbol{\theta_p}$ is above 25 elements. The choice of the γ threshold followed the considerations of [4] coupled with considerations on the exploitation of the dataset (see Section IV).

B. Estimation and uncertainty quantification

The Differential Evolution (DE) and Nelder-Mead (NM) algorithms embedded in the python SciPy library [22] were used to minimize the cost function for parameter estimation. Default options were considered, except from the 'polish' and 'maxiter' options for the DE, that were set at 30 and *True* respectively. The estimates are 'polished' by the NM algorithm till convergence acceptance's default criteria. The serial combination of the two algorithms is a good way to tackle the issue of local minima, but the slow convergence rate of DE restricts it to *offline* estimation problems. The parameters were always scaled to the (1,10) range to improve the performances of the minimization algorithms (and also to compute the *arrival cost* in the model adaptation scheme (see SectionV-C)). The average values $\bar{\mathbf{y}}$ of each data type (i.e. 'Name' column in Table II) were used to normalize simulation errors of different order of magnitudes for the different outputs; it was preferred to the standard L1- and L2-norms as these tend to reduce the relevance of high values of $\mathbf{y}$ (not the best normalization when data are very spiky, as it was in this case). The weights w_y were set to have the same order of magnitude of MRSE% for all the outputs at the first iteration of the minimization problems.

Spearman's coefficient of determination (R^2) and the percentage Mean Absolute Relative Error (MARE (%)) were used to quantify model performances, in light of the consideration in [15].

For the computation of the $\boldsymbol{FIM}$ and related 95% confidence intervals (CI) of the parameter estimates, hypothesis testing and the linear propagation of uncertainty from the parameter estimates to the model outputs, the procedures in [9], [21], [8] were followed. For the weighing matrix in the computation of the $\boldsymbol{FIM}$, a constant relative variance was adopted for the error model: 20% S_{ac} and S_{pro}, and 2%-5% on gas measurements.

For the AM2HN/tan models, all state initial conditions at 15/12/2024 were set consistently with the ones of agri-AcoDM. In the first stage of the AM2HN/tan parameter estimation: (i) all the available correspondences between ADM1- and AM2-like variables were considered [14], as reported in Table I, and (ii) the highly exciting input was obtained varying, within reasonable values based on the industrial practice, both the dilution ratio D (0.015-0.045 d^{-1}) and the diet composition (the fraction of each co-feedstock in the diet was changed up to 40%). In Table II of the main manuscript the 95% CI of $\mathbf{k_h}$ are reported, even though the latter was estimated on synthetic data: this is because $\mathbf{k_h}$ was estimated before the actual stage '(i)' (that exploited all the variable correspondences of Table I), considering the simulation error on the sum of $\mathbf{X_h}$ only. The reason was to limit the effect of N (release) mismatches on its estimate, given the missing salt precipitation in the AM2HN/tan models with respect to agri-AcoDM.

IV. Full-scale applicability: the dataset

The aim of the experiments on the pilot-scale reactors was to reproduce the operating conditions of the full-scale reactor

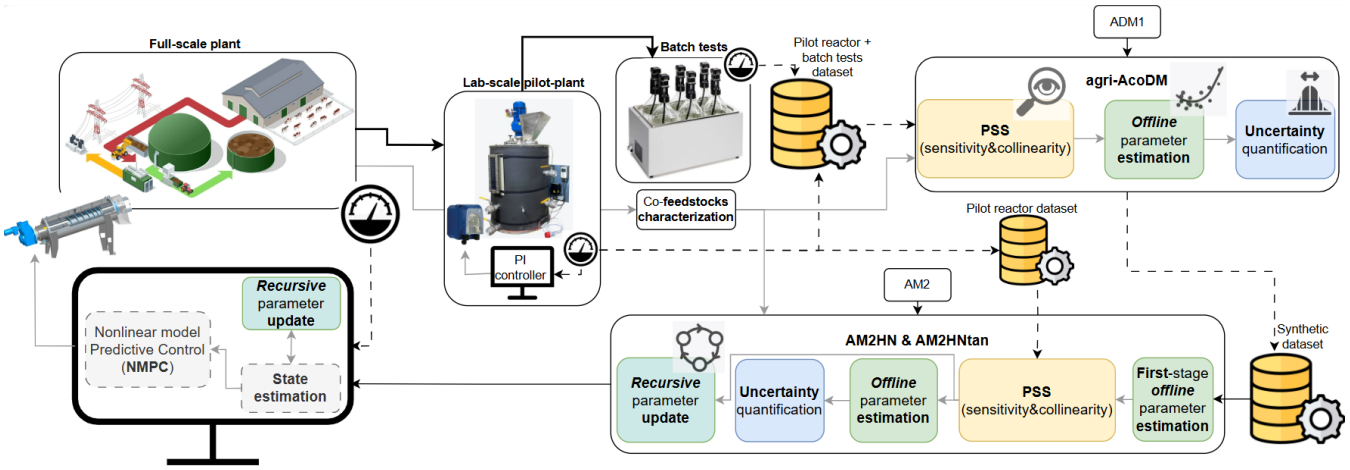

Fig. 1: Visual abstract of the modeling approach followed in this work. Black thick lines represent bacterial inoculum in digestate; black dotted lines represent data, whereas gray lines represent exchange of 'information' in a broader sense; regular black line refers to the reduced-order model that, after the tuning carried out as reported in this work, can be used for the design of state observers and model-based predictive controllers i.e. digital twins.

TABLE I: Variable correspondence and conversion between agri-AcoDM and AM2HN/tan models

	Variable	agri-AcoDM	Conversion*
State variables	$\sum_{i=1}^{n} X_{h,i}$ [g_{VS} L^{-1}]*	$X_{ch,r}, X_{ch,m}, X_{ch,s}, X_{pr,r}, X_{pr,s}, X_{li}$ [g_{COD} L^{-1}]	$\frac{X_{ch,r}+X_{ch,m}+X_{ch,s}}{(COD/VS)_{ch}} + \frac{X_{pr,r}+X_{pr,s}}{(COD/VS)_{pr}} + \frac{X_{li}}{(COD/VS)_{li}}$
	S_1[g_{COD} L^{-1}]	S_{su}, S_{aa}, S_{fa} [g_{COD} L^{-1}]	$S_{su} + S_{aa} + S_{fa}$
	S_2 [mM]	S_{va}, S_{bu}, S_{pro}, S_{ac} [g_{COD} L^{-1}]	$1000 \left(\frac{S_{va}}{208} + \frac{S_{bu}}{160} + \frac{S_{pro}}{112} + \frac{S_{ac}}{64}\right)$
	X_1 [g_{VS} L^{-1}]	X_{su}, X_{aa}, X_{fa} [g_{COD} L^{-1}]	$\frac{X_{su}+X_{aa}+X_{fa}}{(COD/VS)_{bm}}$
	X_2 [g_{VS} L^{-1}]	$X_{ac}, X_{h2}, X_{c4}, X_{pro}$ [g_{COD} L^{-1}]	$\frac{X_{ac}+X_{h2}+X_{c4}+X_{pro}}{(COD/VS)_{bm}}$
	Z [mM]	$S_{va}, S_{bu}, S_{pro}, S_{ac}$ [g_{COD} L^{-1}], S_{co3}, S_{nh3}, S_{oh}, S_h, S_{hpo4}, S_{po4}, S_{h3po4} (M)	$1000\ (\frac{S_{va}}{208} + \frac{S_{bu}}{160} + \frac{S_{pro}}{112} + \frac{S_{ac}}{64} + S_{hco3} + S_{nh3} + 2S_{co3} + S_{oh} - S_h + S_{hpo4} + 2S_{po4} - S_{h3po4})$
	C [mM]	S_{ic} [M]	$1000\ S_{ic}$
	N [mM]	S_{in} [M]	$1000\ S_{in}$
Calculation variables	CO_2 [mM]	S_{CO2} [M]	$1000\ S_{co2}$
	pH [–]	pH [–]	-
	qC [mM d^{-1}]	$\rho_{T,10}$ [M d^{-1}]	$1000\ \rho_{T,10}$
	qM [mM d^{-1}]	$\rho_{T,9}$ [M d^{-1}]	$1000\ \rho_{T,9}$
	Pc [atm]	$P_{gas,co2}$ [bar]	$\frac{P_{gas,co2}}{P_{gas,co2}+P_{gas,ch4}}$
	S_{nh3} [mM]	S_{nh3} [M]	$1000\ S_{nh3}$

*n = number of co-feedstocks in the diet

**COD/VS [ch, pr, li, bm] = [1.18, 1.53, 2.83, 1.41] g_{COD} g_{VS}^{-1}

from which the pilot-scale reactors (12 L working volume reactor, T = 42°C, initial D = 0.031 d^{-1} and organic loading rate (OLR) = 2.84 g_{COD} d^{-1} L^{-1}) were inoculated on the 25/10/2023. Similar loading rate and diet composition (30, 47 and 23% on OLR basis for maize silage, cow slurry and tomato sauce respectively) were maintained at first. Afterward, the dataset entails the control experiment described in [7]. In such experiment the *online* control scheme consisted of equipping the methane flow (Q_{ch4}) controller with an override from the biogas composition (i.e., the CO_2/CH_4 ratio) controller, to guarantee less inhibition-prone transients (as the latter appear to be a fair and cheap *online* proxy of total VFA concentration, better with respect to the *offline* yet cheap 'FOS/TAC' [7]). Due to equipment limitations: i) tomato sauce was fed with the available peristaltic pumps as control action; ii) maize silage and cattle slurry were fed manually and impulsively 3 times a week; iii) the gas composition ($\%CH_4, \%CO_2, \%O_2, H_2S$ in ppm) was analyzed every 3 liters of biogas accumulated in gasbags, whereas the biogas flowrate and pH were logged every minute. To account for this, both models were extended with mass balance equations to reproduce the delay in the measurement of

gas composition caused by gas accumulation in the gasbag. In general, the experimental conditions were a bit more challenging than actual full-scale applications. Tomato sauce was selected to conduct the automatic control experiment as a pumpable substitute for the OLR portion of other TS-rich (i.e. not-pumpable) agro-products and industrial by-products.

In addition to gas data (one-hour-frequent, after raw data manipulation), it is reasonable to assume that some spot (i.e. *offline*) VFA and TAN measurements would be available at full-scale, especially during transients of diet change: *offline* measurements from digestate samples (VS, soluble COD, total COD, TAN, VFA composition) were taken manually 3 times a week, before reactor manual feeding, and in few other occasions. Butirate and valerate were not considered for parameter estimation, as frequently found below the detection limit; VS, soluble and total COD measurements were not exploited too, for other reasons not discussed here for the sake of brevity.

The peculiarity of the entire dataset (15/12/2023-10/04/2024) is that it entails also long reactor free-response (i.e. not-fed reactor/discharge/under-loaded) periods (22/12/2023-08/01/2024; 18-25/03/2024) and impulse responses (in particular, a maize impulse on 26/03/2024), as well as the *transient* dynamic between two different loads and diet compositions (diet change; with respect to the diet applied till 05/02/2024, +53% maize silage feed rate, -27% cow slurry and an average +89% tomato sauce (managed by the controller), were fed after 23/02/2024). Although in practice it is not realistic to have such an informative dataset from continuous full-scale operation, it remains a good general guideline to select a period with different operating conditions for training/calibration, because it tends to prevent overfitting. The test/validation set was also selected crossing different operative conditions to verify for the model's process 'understanding'. Anyway, if the available dataset is actually less comprehensive, modelers can compensate with more batch tests as described below, with limited additional cost to plant owners.

A comprehensive feedstock's characterization (e.g. Weender analysis, Near Infrared Spectroscopy (NIR)) is usually available in full-scale practice, yet with very low frequency, (e.g. seasonal), to follow, coherently, the most relevant variations only. The feedstock characterization was performed as in [6] just once throughout the whole period, with the exception of the measurement of the slurry TS/VS, that was repeated for each stored tank of slurry, and the characterization of tomato sauce, that was mainly taken from the commercial label and completed with one VFA measurement. Some BMP tests were run before the beginning of the pilot-plant operation, inoculated from the reference full-scale reactor, and their data were used to derive the information about the feedstock's biodegradability (BD_{VS}) and a first guess for $\mathbf{k_h}$. The BMP of cow slurry only was repeated on the 10/04/2024, inoculated from the pilot-scale reactor, and exploited along with the others activity tests (same inoculum) in the estimation of the agri-AcoDM's $\boldsymbol{\theta_p}$. All BMP tests were designed according to standardized protocols [17]; the start pH value and the hourly Q_{ch4} were manually and automatically (with AMPTS equipment from BPC Instruments AB, Sweden) recorded respectively. Note that the ideal gas law was used for the conversion between [Q_{ch4},Q_{co2}] (L h^{-1}) to [qM,qC] (mmol L^{-1} d^{-1}).

Table II report a clear picture of the whole dataset and its repartition for different usages. It is important to note that the data of batch tests were used only for the training of the agri-AcoDM, because the initial lag-phase typical of batch tests is likely to be the result of a co-occurrence of different inhibiting factors, so that a highly comprehensive model is needed to fit them. This relevant consideration drove also the author's choice of the γ's upper threshold in the PSS (Section III-A): as specified in the main manuscript, a lower γ threshold was chosen for the AM2HN/tan, due to the practical identifiability (information content) of the dataset without the inclusion of the batch test's data.

V. Results and discussions

In the following text and Tables, the vectorization within square brackets refers to the list of co-feedstocks and its ordering is '[maize silage, cow slurry, tomato sauce]'. The BMP tests conducted before the pilot experimentation resulted in BMP_{∞}= [408, 214, 386] NmL_{CH_4} g_{VS}^{-1} (BD_{VS}= [82, 45, 79]%). The results of the cow slurry BMP test were confirmed by the same test conducted on the 10/04/2024 ($\sim$10% deviation).

A. Agri-AcoDM calibration and performance

Following the results of the PSS, the too rare measurements of TAN resulted in very poor informative content: this implied that no parameters with a strong impact on TAN were selected for estimation. However, even tough TAN was not affected by strong variations during the whole time period, a good fit of its average value is important for the overall estimation task, especially when considering operations that are likely to be prone to S_{nh3} active inhibition. For this reason, before automatic parameter estimation, the TAN data were used for a preliminary manual tuning of the hydrolysis constant of the readily biodegradable proteins ($k_{hyd,xprr}$) only (from 1 down to 0.7 d^{-1}), to obtain a MARE on TAN below 20%. The introduction of salt precipitation and acid-base equilibrium non-ideality revealed to be particularly beneficial for matching the pH at the beginning of batch activity tests, and this is of particular interest to correctly grasp the initial lag-phase typical of these tests. Note that, since precipitation is in place, caution has to be paid in the exploitation of inorganic compound measurements (e.g. TAN and partial/total alkalinity), because the handling of samples (e.g. dilution) has a strong impact: it is thus advised that modelers do take into account the dilution ratios of these measurements in their models before computing simulation errors, and that the model tuning guidelines in [2] are followed.

For the estimation, the different output weights w_y = [Q_{ch4}, Q_{co2}, S_{ac}, S_{pro}, $Q_{ch4,Ac3}$, $Q_{ch4,Ac10}$, $Q_{ch4,Pro3}$, $Q_{ch4,Pro6}$, $Q_{ch4,BMPslurry}$] were set to [40, 40, 4, 4, 1, 10, 2, 2, 4]. The

TABLE II: Summary of the measurements included in the dataset and their different exploitation

Name	Unit	Type	Experiment type**	Ny	Date	Exploitation
$\mathbf{Q_{ch4}}$	L h^{-1}	*online*	pilot	840	15.12.2023-19.01.2024	test
$\mathbf{Q_{ch4}}$	L h^{-1}	*online*	pilot	1968	19.01.2024-10.04.2024	training
$\mathbf{Q_{ch4}}$	L h^{-1}	*online*	batch activity $S_{ac,0}$* = 3 g L^{-1}	408	10.04.2024-27.04.2024	training
$\mathbf{Q_{ch4}}$	L h^{-1}	*online*	batch activity $S_{ac,0}$ = 10 g L^{-1}	408	10.04.2024-27.04.2024	training
$\mathbf{Q_{ch4}}$	L h^{-1}	*online*	batch activity $S_{pro,0}$ = 3 g L^{-1}	408	10.04.2024-27.04.2024	training
$\mathbf{Q_{ch4}}$	L h^{-1}	*online*	batch activity $S_{pro,0}$ = 6 g L^{-1}	408	10.04.2024-27.04.2024	training
$\mathbf{Q_{ch4}}$	L h^{-1}	*online*	batch BMP cow slurry	408	10.04.2024-27.04.2024	training
$\mathbf{Q_{co2}}$	L h^{-1}	*online*	pilot	840	15.12.2023-19.01.2024	test
$\mathbf{Q_{co2}}$	L h^{-1}	*online*	pilot	1'968	19.01.2024-10.04.2024	training
$\mathbf{S_{ac}}$	mg L^{-1}	*offline*	pilot	10	15.12.2023-19.01.2024	test
$\mathbf{S_{ac}}$	mg L^{-1}	*offline*	pilot	62	19.01.2024-10.04.2024	training
$\mathbf{S_{pro}}$	mg L^{-1}	*offline*	pilot	10	15.12.2023-19.01.2024	test
$\mathbf{S_{pro}}$	mg L^{-1}	*offline*	pilot	62	19.01.2024-10.04.2024	training
TAN	mg_N L^{-1}	*offline*	pilot	18	15.12.2023-10.04.2024	manual tuning
pH	-	*online*	pilot	2'808	15.12.2023-10.04.2024	test

*The initial concentration of the specific substrate is reported for batch activity tests.
**Dynamic Q_{ch4} data from batch tests were used only for the training of the agri-AcoDM (see Section IV).

subscript of the different Q_{ch4} data refers to the different batch tests (e.g. the activity tests are identified by the subscript: 'substrate type, substrate's initial concentration' as specified in Table II).

The overall gas-liquid mass transfer coefficient (k_{La}) of the pilot-scale reactor was not considered for estimation, since a reliable value was measured by O_2-saturation test (equal to 10 d^{-1} at the actual reactor stirring mode). The quite low k_{La} of batch tests ($k_{La,batch}$) that was estimated may be reasonable, considering the slow and discontinuous mixing of the experimental setup, but it is always advisable to validate it with dedicated saturation tests.

The CI of VFAs (S_{ac} and S_{pro}) appeared to be very sensitive to the relative variance assumed for the error model.

B. AM2HN/tan calibration and performance

Results from the first-stage estimation (i.e. on synthetic data) of the reduced-order models were very satisfactory: R^2 was always higher than 0.6, reaching 0.97 for X_1. AM2HN was better over X_1, whereas AM2HNtan was better over X_2 and S_2. For inorganic C and total alkalinity (Z), R^2 was higher than 0.6, but an average offset of 30% was present, which is explained by the missing salt precipitation with respect to agri-AcoDM. This didn't cause any loss of performance over the model outputs, primarily because Q_{co2} is a function of the C and Z difference. The 'inner' (i.e. farer in the cascade of the AD reactions from the available measurable quantities) stoichiometric parameters (k_1, k_2, k_3) were not included in the PSS scheme to be possibly 'refined' on real data: the modeling and estimation approach that was followed indeed trusts agri-AcoDM for the estimation of parameters that strongly affect the trajectories of states but for which no validation data are available (namely X_1, X_2 and S_1). Figure 2 reports the Haldane curves on VFA evaluated with the estimated parameter values, for all the models involved. For both AM2HNN/tan, the curves have similar total VFA's (S_2) optimal value (on the x-axis of the Haldane function) compared to the one on S_{ac} in agri-AcoDM (difference $\leq$ 30%), but the maximum methanogenesis Haldane's rate (on the y-axis of the Haldane function) is lower (difference up to 70%). This can be due to X_2 lumping different bacterial populations and not only X_{ac}. Moreover, as expected, the maximum methanogenesis Haldane's rate in AM2HNtan is higher compared to the one in AM2HN, since the Haldane rate is further reduced by free ammonia inhibition to compute the actual kinetic rate μ_2 in AM2HNtan.

C. Recursive model adaptation: AM2HN parameter update

In [11], two possibilities of model adaptation schemes are considered if model mismatch increases *online* during operation: (i) a data-driven model of the residuals is added in a parallel hybrid modeling scheme when the system input varies substantially with respect to the previous working conditions, whereas (ii) if the system input did not change, model parameters are re-estimated/updated. In this work, the AM2HN/tan models were built to have a sufficient prediction capability for reasonably different input conditions, so that the '(ii)' case was considered.

In the prospective of the design of a nonlinear model predictive controller (NMPC), the aforementioned approach was tested in view of the asynchronous (i.e. with different frequency) separation between unmeasured state and parameter *online* estimations, that can be beneficial with respect to a unique exogenous state observer (e.g. Extended Kalman Filter (EKF) with state vector augmented with practically identifiable parameters such as $\mu_{max,2}$); otherwise, the risk is to follow too much the measurement noise or to 'absorb' the measurement information on the parameter instead of on the state estimates, especially if strong collinearity between

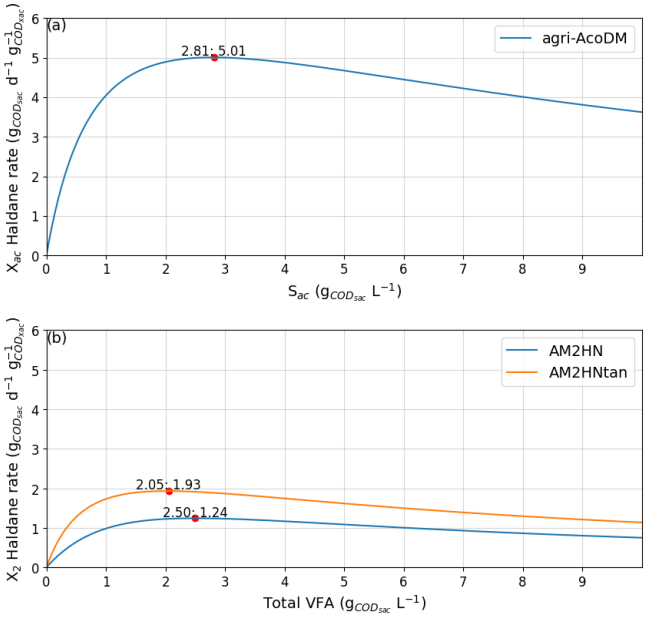

Fig. 2: Haldane's curve with the parameters $\boldsymbol{\theta}^*_{PSS}$ estimated *offline*: (a) for agri-AcoDM (corrected with temperature = 316.15 K) and (b) for AM2HN and AM2HNtan (values converted to acetate-equivalent, agri-AcoDM-like, units).

states and parameters exists on the output measurements (e.g. $\mu_{max,2}$ and X_2 on qM). In fact, if the model is designed with enough 'physics-based' prediction ability, it is reasonable to assume that parameters may change, yet with lower frequency compared to states. This holds especially for biological systems.

In this work, model's parameters were updated over 10-days-long time windows of the pilot-scale data (sliding, but not overlapping): the width of such time windows was selected based on the system's characteristic time of response.

The *arrival cost* that was added to the cost function plays a role similar to the one of the PSS scheme in reducing the risk of overfit and it is effective in recursive schemes where, compared to *offline* estimations, the need for *exploration* is generally lower than the one for *exploitation* of the parameter values learned on old data and/or *offline*. Compared to [23], a more naive yet intuitive weighting ($\mathbf{W}_\theta$) based on the local relative-relative sensitivity ranking indexes computed on the k^{th} time window was applied to the *arrival cost*. The main drawback of this approach is its dependence on user-configurable 'hyperparameters' such as: (i) the w_y relative weights of the different outputs in the sum of the simulation errors' term of the cost function (J_k), and (ii) the mapping function for each parameter of $\boldsymbol{\theta_p}$ from its $\mathbf{SI_{rr}}_{,k}$'s ranking index to its diagonal element of $\mathbf{W}_\theta$ in the *arrival* cost term of the cost function. An affine linear mapping (Eq.(26)) was selected with user-configurable intercept and slope (a,b). Indeed, $\mathbf{W}_\theta$ is a square diagonal matrix with the j^{th} element defined as:

$$w_{j,j} = a + b\rho_{j,k} \tag{26}$$

where $\rho_{j,k}$ is the index of the $\boldsymbol{\delta}^{msqr}$ metric of the parameter $\theta_{p,j}$ in the $\mathbf{SI_{rr}}_{,k}$ ranking, evaluated on the k^{th} time window (i.e. an element of the ranking indexes vector $\boldsymbol{\rho}_k \in \mathbb{R}^{dim(\boldsymbol{\theta}_p)}$). In this work, a and b were set to 10 and 30 respectively to obtain similar order of magnitudes for the different terms of the cost function at the beginning of the optimization on the first time window, if the initial guess of $\boldsymbol{\theta}^*_{\mathbf{p},1}$ is set randomly from the Gaussian distributions of the $\boldsymbol{\theta}^*_{\mathbf{p}}$ learned *offline* ($\mathcal{N}$(*expected values*, standard deviations)). The use of Sobol's sensitivity computed within narrow bounds from the reference/previous parameter values is expected to lead to more robust results, but it was not selected for *on-line*/recursive purposes due to its high computational burden. The most useful information that can be extracted by this approach is a mapping F between the parameters and the states, outputs and/or inputs ($\boldsymbol{\theta_p}(t) = F(\mathbf{x}(t), \mathbf{y}(t), \mathbf{u}(t))$), but much more data would be required to obtain a statistically meaningful map, to the authors' opinion.

After some preliminary tests, some unsensitive parameters were discarded and only $k_4, k_5, k_6, \mu_{max,2}, K_{s,2}, K_{2,I}$ and $k_{d,2}$ were considered for update. Although $\mu_{max,2}$ is the parameters that seemed to trigger the most the model adaptation to the total VFA (S_2) transient, the combination with some small variations of $K_{s,2}$ may have played a role. However, the high collinearity between $\mu_{max,2}$ and $K_{s,2}$ suggests to update one or the other only. The improvement/deterioration of 'posterior' (model simulated with $\boldsymbol{\theta}^*_{\mathbf{p},k}$) and 'prior' (model simulated with $\boldsymbol{\theta}^*_{\mathbf{p},k-1}$) fitting is on average less relevant for Q_{ch4} and CO_2/CH_4 ($\leq$ 15%) with respect to S_2, but this result may depend on the choice of the w_y.

In the prospective of the design of a NMPC, although 'prior' model trajectories presented a worse fitting over some windows, the update could be beneficial to prevent overloading the system e.g. on the 4^{th} and 5^{th} windows, where S_2 accumulation is foreseen (the 'bad' 'prior' would be then corrected by the state observer). With this in mind, slack variables will be needed to guarantee recursive feasibility if an upper bound on S_2 is enforced as state constraint, for safety.

VI. Conclusions

Further works are summarized below:

- Testing PSS methods that better deal with the true (i.e. not-Gaussian) uncertainty probability distribution (e.g. profile likelihood) will be carried out on the same dataset for a fair comparison [18].
- State observer's design, in which it will be of relevance the ability to exploit the precious *offline* VFA measurements too, so that multi-rate EKF or moving-horizon estimators (MHE) will be considered. Alternatively, a parallelization between a state observer that considers only the *online* data and a parameter update scheme as the one proposed in this work will be studied.
- The ultimate goal is the design and validation of a robust NMPC scheme able to improve the control performances with respect to the results obtained testing the classical control scheme described in [7], over similar

diet change: indeed, good tracking performance and controlled Q_{ch4} improvement was achieved after the period of diet change, but the tracking was poor on the transient because of the inability of the classical control to foresee process inhibition.

REFERENCES

[1] Juan C. Acosta-Pavas, Carlos E. Robles-Rodríguez, Jérôme Morchain, Claire Dumas, Arnaud Cockx, and César A. Aceves-Lara. Dynamic modeling of biological methanation for different reactor configurations: An extension of the anaerobic digestion model No. 1. *Fuel*, 344:128106, 2023.

[2] Damien Batstone and Xavier Flores-Alsina. *Generalised Physicochemical Model (PCM) for Wastewater Processes*. IWA Publishing, 11 2022.

[3] D.J. Batstone, J. Keller, I. Angelidaki, S.V. Kalyuzhnyi, S.G. Pavlostathis, A. Rozzi, W.T.M. Sanders, H. a Siegrist, and V.A. Vavilin. The iwa anaerobic digestion model no 1 (ADM1). *Water Science and technology*, 45(10):65–73, 2002.

[4] Roland Brun, Peter Reichert, and Hans R. Künsch. Practical identifiability analysis of large environmental simulation models. *Water Resources Research*, 37(4):1015–1030, 2001.

[5] K Bułkowska, I Białobrzewski, E Klimiuk, and T Pokoj. Kinetic parameters of volatile fatty acids uptake in the ADM1 as key factors for modeling co-digestion of silages with pig manure, thin stillage and glycerine phase. *Renewable Energy*, 126:163–176, 2018.

[6] D. Carecci, A. Catenacci, S. Rossi, F. Casagli, G. Ferretti, A. Leva, and E. Ficara. A plant-wide modelling framework to describe microalgae growth on liquid digestate in agro-zootechnical biomethane plants. *Chemical Engineering Journal*, 485:149981, 2024.

[7] Davide Carecci, Arianna Catenacci, Elena Ficara, Gianni Ferretti, and Alberto Leva. Modelling, optimisation and control of full-scale co-digestion biomethane plants. In *Proceedings of the 63rd IEEE Conference on Decision and Control*. IEEE, in press, 2024.

[8] Francesca Casagli, Gaetano Zuccaro, Olivier Bernard, Jean-Philippe Steyer, and Elena Ficara. ALBA: A comprehensive growth model to optimize algae-bacteria wastewater treatment in raceway ponds. *Water Research*, 190:116734, 2021.

[9] A. Catenacci, D. Carecci, A. Leva, A. Guerreschi, G. Ferretti, and E. Ficara. Towards maximization of parameters identifiability: Development of the calopt tool and its application to the anaerobic digestion model. *Chemical Engineering Journal*, 499:155743, 2024.

[10] Audrey Chai, Yee-Shian Wong, Soon-An Ong, Nabilah Aminah Lutpi, Sung-Ting Sam, Wei-Chin Kee, and Hock-Hoo Ng. Haldane-andrews substrate inhibition kinetics for pilot scale thermophilic anaerobic degradation of sugarcane vinasse. *Bioresource technology*, 336:125319, 2021.

[11] Laura Boca de Giuli, Alessio La Bella, Giuseppe De Nicolao, and Riccardo Scattolini. Lifelong learning for monitoring and adaptation of data-based dynamical models: A statistical process control approach. In *2024 European Control Conference (ECC)*, pages 947–952, 2024.

[12] Xavier Flores-Alsina, Kimberly Solon, Christian Kazadi Mbamba, Stephan Tait, Krist V. Gernaey, Ulf Jeppsson, and Damien J. Batstone. Modelling phosphorus (P), sulfur (S) and iron (Fe) interactions for dynamic simulations of anaerobic digestion processes. *Water Research*, 95:370–382, 2016.

[13] P. Fritzson, A. Pop, K. Abdelhak, A. Asghar, B. Bachmann, W. Braun, D. Bouskela, R. Braun, L. Rogovchenko-Buffoni, F. Casella, R. Castro, R. Franke, D. Fritzson, M. Gebremedhin, A. Heuermann, B. Lie, A. Mengist, L. Mikelsons, K. Moudgalya, and P. Östlund. The OpenModelica Integrated Environment for Modeling, Simulation, and Model-Based Development. *Modeling, Identification and Control: A Norwegian Research Bulletin*, 41:241–295, 10 2020.

[14] S. Hassam, E. Ficara, A. Leva, and J. Harmand. A generic and systematic procedure to derive a simplified model from the anaerobic digestion model No. 1 (ADM1). *Biochemical Engineering Journal*, 99:193–203, 2015.

[15] H. Hauduc, M.B. Neumann, D. Muschalla, V. Gamerith, S. Gillot, and P.A. Vanrolleghem. Efficiency criteria for environmental model quality assessment: A review and its application to wastewater treatment. *Environmental Modelling & Software*, 68:196–204, 2015.

[16] Jon Herman and Will Usher. Salib: An open-source python library for sensitivity analysis. *Journal of Open Source Software*, 2(9):97, 2017.

[17] Christof Holliger, Madalena Alves, Diana Andrade, Irini Angelidaki, Sergi Astals, Urs Baier, Claire Bougrier, Pierre Buffière, Marta Carballa, Vinnie de Wilde, Florian Ebertseder, Belén Fernández, Elena Ficara, Ioannis Fotidis, Jean-Claude Frigon, Hélène Fruteau de Laclos, Dara S. M. Ghasimi, Gabrielle Hack, Mathias Hartel, Joern Heerenklage, Ilona Sarvari Horvath, Pavel Jenicek, Konrad Koch, Judith Krautwald, Javier Lizasoain, Jing Liu, Lona Mosberger, Mihaela Nistor, Hans Oechsner, João Vítor Oliveira, Mark Paterson, André Pauss, Sébastien Pommier, Isabella Porqueddu, Francisco Raposo, Thierry Ribeiro, Florian Rüsch Pfund, Sten Strömberg, Michel Torrijos, Miriam van Eekert, Jules van Lier, Harald Wedwitschka, and Isabella Wierinck. Towards a standardization of biomethane potential tests. *Water Science and Technology*, 74(11):2515–2522, 09 2016.

[18] Kevin A. P. McLean and Kim B. McAuley. Mathematical modelling of chemical processes—obtaining the best model predictions and parameter estimates using identifiability and estimability procedures. *The Canadian Journal of Chemical Engineering*, 90(2):351–366, 2012.

[19] Rongrong Mo, Wenjie Guo, Damien Batstone, Jacek Makinia, and Yongmei Li. Modifications to the anaerobic digestion model no. 1 (ADM1) for enhanced understanding and application of the anaerobic treatment processes – a comprehensive review. *Water Research*, 244:120504, 2023.

[20] George Qian and Adam Mahdi. Sensitivity analysis methods in the biomedical sciences. *Mathematical Biosciences*, 323:108306, 2020.

[21] Alberto Saccardo, Beatriz Felices-Rando, Eleonora Sforza, and Fabrizio Bezzo. Droop model identification via model-based design of experiments to describe microalgae nitrogen uptake in continuous photobioreactors. *Chemical Engineering Journal*, 468:143577, 2023.

[22] Rainer Storn and Kenneth Price. Differential evolution – a simple and efficient heuristic for global optimization over continuous spaces. *J. of Global Optimization*, 11(4):341–359, dec 1997.

[23] Andrea Tuveri, Caroline S.M. Nakama, José Matias, Haakon Eng Holck, Johannes Jäschke, Lars Imsland, and Nadav Bar. A regularized moving horizon estimator for combined state and parameter estimation in a bioprocess experimental application. *Computers & Chemical Engineering*, 172:108183, 2023.

[24] Sören Weinrich, Eric Mauky, Thomas Schmidt, Christian Krebs, Jan Liebetrau, and Michael Nelles. Systematic simplification of the anaerobic digestion model No. 1 (ADM1) – laboratory experiments and model application. *Bioresource Technology*, 333:125104, 2021.

[25] Sören Weinrich and Michael Nelles. Systematic simplification of the anaerobic digestion model No. 1 (ADM1) – model development and stoichiometric analysis. *Bioresource Technology*, 333:125124, 2021.